

Temperature and humidity retrieval from simulated Infrared Atmospheric Sounding Interferometer (IASI) measurements

Jeffrey A. Lerner,¹ Elisabeth Weisz,² and Gottfried Kirchengast

Institute for Geophysics, Astrophysics, and Meteorology (IGAM), University of Graz, Graz, Austria

Received 28 August 2000; revised 13 August 2001; accepted 15 August 2001; published 17 July 2002.

[1] An efficient temperature and humidity retrieval algorithm for radiometric measurements at high spectral resolution is introduced and applied to climatological profiles. The algorithm is developed for analyzing Infrared Atmospheric Sounding Interferometer (IASI) data of the European weather satellite METOP-1 (launch scheduled 2005) for climatological purposes but is also applicable for other purposes and to other similar data. The algorithm's core features are a channel selection methodology followed by a linearized optimal estimation. The key concept of the former is that a small subset (5–10%) of all available IASI channels (~8000) is selected based on maximizing a suitable information content measure at each retrieval level. This enables efficiency and robustness of the retrieval algorithm and curtails the high redundancy in the measurements. In addition to profile and error covariance estimates optimal estimation furnishes various sensitivity functions of which we used "weighting functions" for quantifying the utility of measurement channels and "averaging kernel functions" for assessing the resolution of retrieved profiles. Results based on simulated IASI spectra computed from a set of standard climatological profiles and a realistic radiometric noise model demonstrate, for clear air, the capabilities of high spectral resolution measurements for improving temperature and humidity soundings compared to current operational sensors. In the troposphere (below ~200 hPa), retrieved profiles exhibit temperature errors of <1 K and specific humidity errors of <10% at most heights, associated with a vertical resolution of ~1.5–2 km. Promising performance was found in the upper troposphere (500–200 hPa), where about five independent reliable values of temperature and humidity are available indicating the high potential of the IASI sensor for monitoring climatic changes in upper tropospheric moisture. Tests on the sensitivity of retrieved profiles to the quality of a priori profiles showed weak sensitivity of temperature but significant sensitivity of humidity. The results provide a solid basis and clear guidance for improvements of the presented algorithm for reliable large-scale application on cloud-free spectra.

INDEX TERMS: 0394 Atmospheric Composition and Structure: Instruments and techniques; 3394 Meteorology and Atmospheric Dynamics: Instruments and techniques; 0365 Atmospheric Composition and Structure: Troposphere—composition and chemistry; 0340 Atmospheric Composition and Structure: Middle atmosphere—composition and chemistry; *KEYWORDS:* IASI, Interferometer, temperature retrieval, water vapor retrieval, channel selection

1. Introduction

[2] The determination of atmospheric humidity and temperature profiles from satellite measurements has a history dating back to the early 1970s with the NIMBUS series of operational weather satellites. In the last two decades, improvements have been made on the horizontal sampling and accuracy of retrievals particularly with instruments such

as the High Resolution Infrared Sounder (HIRS) [Kidwell, 1986]. The numerical weather prediction (NWP) and climate monitoring communities both require improvements in both accuracy (<1 K for temperature and <10% for humidity in the troposphere) and vertical resolution (1–2 km under cloud-free conditions) of satellite soundings to meet their objectives [World Meteorological Organization, 1998]. It appears that these requirements may be met with the launch of satellites carrying interferometers, which sample the thermal infrared spectrum at high resolution (<0.5 cm⁻¹).

[3] The concept of obtaining high vertical resolution profiles from high spectral resolution interferometers was discussed by Kyle [1977] and Smith *et al.* [1979], among others. They proposed the use of a partial interferogram for

¹Now at Fleet Numerical Meteorology and Oceanography Center, Monterey, California, USA.

²Now at CIMSS/Space Science and Engineering Center, University of Wisconsin, Madison, Wisconsin, USA.

high-resolution temperature soundings with the capability of better than 1 K accuracy. Despite the coarse horizontal resolution, the Infrared Interferometer Spectrometer (IRIS) on the NIMBUS 3/4 satellites offered a glimpse into the utility of interferometric data for temperature, water vapor, and other trace gas retrievals from space. More recently, the aircraft High-resolution Interferometer Spectrometer (HIS) instruments [Smith *et al.*, 1993] have demonstrated the ability to sample the horizontal structure of temperature and humidity throughout the middle and upper troposphere from aircraft. The Atmospheric Infrared Sounder (AIRS) is a high-resolution grating spectrometer that will be launched on the AQUA satellite in 2001. It will sample several infrared absorption bands useful for temperature and humidity retrievals. The Infrared Atmospheric Sounding Interferometer (IASI) is a Michelson-type interferometer sampling the entire thermal infrared spectrum from 3.6 to 15 μm and is scheduled to fly aboard the METOP-1 satellite in 2005 (CNES, Infrared Atmospheric Sounding Interferometer homepage, available at <http://smc.cnes.fr/IASI/index.html>, hereinafter referred to as IASI homepage). The Cross-track Infrared Sounder (CrIS) is another future high-spectral resolution interferometer system being developed for the National Polar-Orbiting Operational Environmental Satellite System (NPOESS) with the 1st launch foreseen also in 2005 on the NPOESS Preparatory Program (NPP) satellite.

[4] One of the primary objectives of the IASI instrument, according to the IASI Science Plan (available at <http://smc.cnes.fr/IASI/index.html>), is to improve the vertical resolution of temperature and water vapor profiles to ~ 1 km in the middle to lower troposphere and to improve the retrieval accuracy to within 1 K in temperature and 10% in (specific) humidity. Part of the scientific motivation for accomplishing this stems from the key role of water vapor in the upper troposphere and its effects on the global climate since only small changes in water vapor and its trends have serious implications on the amount of thermal energy escaping to space [Schmetz *et al.*, 1995; Spencer and Braswell, 1997]. Improved quantification of global climate variability is another important theme that advanced sounder retrievals will likely be able to address, particularly contributing to our knowledge of the climate of the upper troposphere. In addition, NWP will greatly benefit from more accurate and frequent temperature and humidity profiles for operational and research needs.

[5] The fundamental problem of inverting the radiative transfer equation to retrieve the state of the atmosphere, which produced the corresponding observation (radiance or brightness temperature), is an ill-posed problem such that there exists no unique solution. Rodgers [2000] presents a comprehensive tutorial on retrieval theory and outlines many of the various methods on approaching the under-determined, nonlinear problem of geophysical retrievals.

[6] In this paper, temperature and humidity profiles are retrieved from simulated IASI measurements using a set of standard climatological profiles (U.S. standard atmosphere profiles). Section 2 describes how measurements from the IASI instrument are simulated as well as the retrieval algorithm including the channel selection procedure and the optimal estimation methodology used. The results and corresponding discussion of applying the retrieval algorithm and performing various sensitivity tests is presented in

section 3. A summary and conclusions are given in section 4, where also avenues of useful further improvements are outlined.

2. IASI Data Simulation and Retrieval Methodology

2.1. Sensor and Satellite

[7] The European meteorological operational satellite METOP-1 carrying the IASI sensor is scheduled to be launched in 2005 as the initial component of the European Polar System (EPS) operated by the European Organization for the Exploitation of Meteorological Satellites, EUMETSAT (IASI homepage). It is the first in a series of European polar orbiting satellites dedicated to operational meteorology and climate monitoring. The satellite will orbit Earth at an altitude of ~ 830 km in a 5-day repeat sun-synchronous orbit with a 0930 local time of equator crossing. In addition to the novel IASI instrument, companion meteorological payload instruments will include the Advanced Microwave Sounding Unit A (AMSU-A) and the High-Resolution Infrared Sounder (HIRS/3), which are already in orbit on the U.S. weather satellite NOAA-15.

[8] IASI is a high spectral resolution Michelson-type interferometer detecting thermal emissions from a spectral range between 645–2760 cm^{-1} with a constant spectral sampling interval at 0.25 cm^{-1} . The unapodized spectral resolution varies slightly with wavelength between ~ 0.32 – 0.42 cm^{-1} (apodized spectral resolution is 0.5 cm^{-1}). The radiance spectrum is obtained by taking the Fourier transform of the sampled interferogram. The cross-track scanning mode of IASI is similar to its companion METOP payload instruments mentioned in the previous paragraph. The swath width is approximately ± 1100 km with an instantaneous field of view (IFOV) of $\sim 48 \times 48$ km at nadir corresponding to one observation pixel, which in turn is composed of 2×2 IASI detector pixels with ~ 12 km diameter. Each swath is covered, in “step-and-dwell mode,” by 30 full pixels acquired within ~ 8 s. More details on the sensor is available at <http://smc.cnes.fr/IASI/index.html>.

2.2. Forward Modeling

[9] For the successful retrieval of temperature or humidity within the framework of an optimal estimation approach as adopted here, the underlying physics of the measurement need be properly modeled by a forward model solving the radiative transfer equation. At the same time, proper modeling of the derivative of the forward model with respect to the state (also termed “weighting matrix” or “Jacobian”) is quite important, especially with regard to computational efficiency, since nonlinearities in the problem of interest demand an iterative state estimation. The general forward model equation mapping the state (atmospheric profile) into measurement space (satellite-measured radiance or brightness temperature spectrum) takes the form [e.g., Rodgers, 2000]

$$\mathbf{y} = \mathbf{F}(\mathbf{x}) + \epsilon, \quad (1)$$

where \mathbf{y} is the measurement vector, $\mathbf{F}(\mathbf{x})$ is the forward model operator for a given state \mathbf{x} , and ϵ is the measurement error. The measurement error characteristics should be

known in terms of systematic biases and random instrument noise. The measurements \mathbf{y} should in fact be corrected for biases before using them in the retrieval so that ϵ can be statistically well characterized by a measurement error covariance matrix (see section 2.4). Inserting reasonable temperature and humidity test profiles for \mathbf{x} , (1) was used to confirm that the present retrieval problem is moderately nonlinear only so that we can apply (1) in linearized form, i.e., replace $\mathbf{y} = \mathbf{F}(\mathbf{x})$ by $(\mathbf{y} - \mathbf{y}_0) = \mathbf{K}_0(\mathbf{x} - \mathbf{x}_0)$, where $\mathbf{K}_0 = \partial\mathbf{F}(\mathbf{x})/\partial\mathbf{x}$ is the weighting matrix (evaluated at state \mathbf{x}_0) and \mathbf{x}_0 is a suitable reference state [Rodgers, 2000].

[10] For computing $\mathbf{F}(\mathbf{x}) = \mathbf{T}_B$ (\mathbf{T}_B , brightness temperature) and \mathbf{K}_0 , the fast radiative transfer model RTIASI [Matricardi and Saunders, 1999; P. Schluessel, EUMETSAT, private communications, 2000] was used, which can take temperature and humidity (and other) profiles as input and then furnishes simulated IASI brightness temperature measurements and temperature and humidity weighting matrices for any desired subset of IASI channels. The model calculates level-to-space transmittances on 43 pressure levels spanning from 0.1 hPa (~ 65 km height) to the surface. We use these same levels, the so-called “ATOVS pressure level grid,” also as our retrieval grid (all 43 levels for temperature, the lowest 28 levels for humidity). Convolved line-by-line (LBL) transmittances from a set of atmospheric profiles and selected predictors are used by RTIASI to compute regression coefficients in turn used to derive approximate transmittances from which the final estimates of brightness temperatures (or radiances) are made. In comparison with LBL model calculations, RTIASI performs at or below a noise of <0.5 K for wave numbers below ~ 2400 cm^{-1} [Matricardi and Saunders, 1999]. An example of brightness temperatures computed by the RTIASI model for a standard midlatitude summer atmosphere is displayed in Figure 1. The results for all channels of IASI are depicted and major spectral features such as the 15 μm CO_2 band, 9.6 μm O_3 band, and 6.3 μm H_2O band are easily identifiable.

2.3. Channel Reduction Procedure

[11] For each individual IFOV pixel, full IASI spectra will contain 8461 channels from 645 – 2760 cm^{-1} with 0.25 cm^{-1} channel width, which is an enormous amount of data. For the retrieval of temperature and humidity, it is not practical nor an advantage to use all spectral points [e.g., Rodgers, 1996]. Therefore a strategy is devised to eliminate those channels whose information content does not add to the final retrieval accuracy and, even before for the sake of efficiency, those channels potentially contaminated by solar radiation or significantly affected by “foreign” trace gases (not required for temperature and humidity profiling but posing difficulties in forward modeling). Subsections 2.3.1 to 2.3.4 subsequently discuss the reduction measures applied in our algorithm.

2.3.1. Elimination of wavelength <4 μm channels

[12] As a first filter based on evaluating the general utility of the channels for the intended purpose, all channels with wave numbers >2500 cm^{-1} (wavelengths <4 μm) are dropped, which reduces the number of channels from 8461 to ~ 7420 . The removal of these channels avoids potential problems with contamination by residual short-wave (solar) radiation, which plays some role up to ~ 4 μm

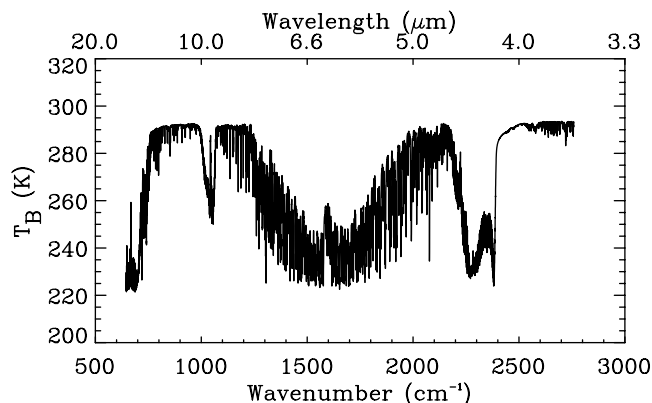


Figure 1. Simulated IASI brightness temperature spectrum for a standard midlatitude summer atmosphere.

but is not taken into account by the RTIASI forward model. Moreover, the eliminated channels, mostly surface channels or channels with some CH_4 sensitivity, are not missed in the temperature and humidity profiling context. Retaining the channels for test purposes in the procedure described in subsection 2.3.3 below showed that they would not be selected anyway because of the comparatively high IASI radiometric noise at wave numbers >2500 cm^{-1} (e.g., IASI homepage). Thus they might also be dropped simply for increasing the efficiency of that procedure.

2.3.2. “Foreign” gas elimination

[13] Including channels with significant emissions from variable trace gas species other than the ones best aiding temperature and humidity retrieval (CO_2 , H_2O , partially N_2O) increases the uncertainty in the retrieved states in the present study, because these variable gases are treated as fixed, partly due to limitations of the RTIASI model. With the luxury of kilo channel availability, we remove those channels which have significant contribution from such “foreign” trace gases including O_3 , CH_4 , CO , and (in the “atmospheric window” region) CFCs (chlorofluorocarbons). Also most of the “atmospheric window” region is dropped as not a high number of such channels is required for the intended vertical profiling. Based on careful consideration of the relevant “foreign” absorption features within the range of interest the eliminated spectral regions include the following: 825 – 1100 cm^{-1} (9.1 – 12.1 μm ; “atmospheric window”, O_3 , CFCs), 1220 – 1370 cm^{-1} (7.3 – 8.2 μm ; CH_4), and 2085 – 2220 cm^{-1} (4.5 – 4.8 μm ; CO , O_3), respectively. Figure 2 shows these excluded areas as shaded regions. We confirmed via sensitivity tests including these bands (and assuming known “foreign” gas concentrations) that their exclusion does not degrade the temperature and humidity profiling performance. After the removal of the “foreign” bands we are left with groups of channels in preferred absorption bands such as the ~ 650 cm^{-1} CO_2 band, the ~ 1600 cm^{-1} H_2O band, and the ~ 2250 cm^{-1} $\text{CO}_2/\text{N}_2\text{O}$ band. This step reduces the number of potential retrieval channels by ~ 2240 channels ($\sim 26\%$ of the original set).

2.3.3. Information content based channel selection

[14] As we are still left with over 5000 channels at this point, a way is now needed to reduce this abundance of channels by prioritizing in some way part of the measure-

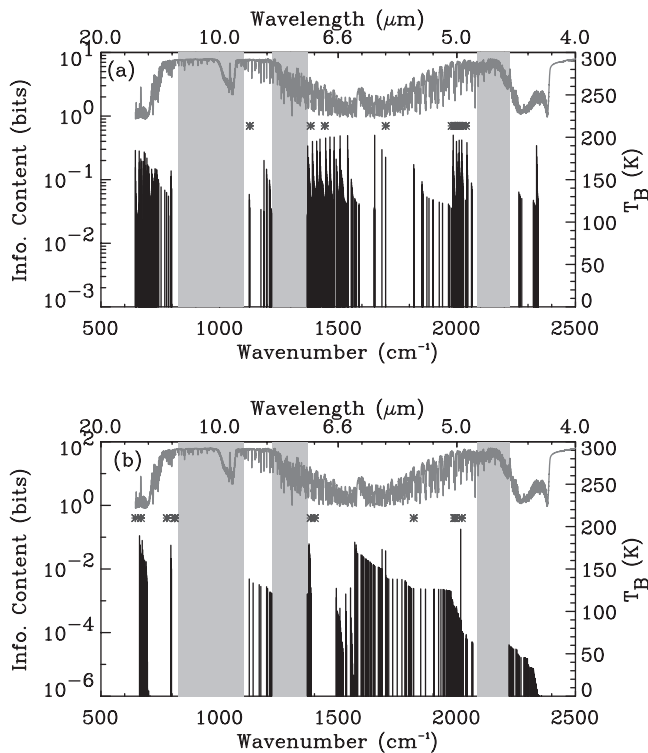


Figure 2. Information content (IC) based channel distribution and IC magnitude (vertical spikes in units bits) for (a) temperature and (b) humidity. Shaded areas indicate bands excluded due to significant “foreign” gas contributions. Asterisk symbols indicate pseudo channels, i.e., channels derived from clustering of neighboring channels. On top of each panel the midlatitude summer atmosphere brightness temperature, T_B , spectrum is drawn for reference.

ments over other parts. We found it a sensible approach, and a key to an efficient and robust algorithm, to perform this reduction based on two ingredients: (1) a measure for the information which a given channel will supply to the retrieval at a given pressure level and (2) a formulation for a target number of channels not yet implying a cost in retrieval accuracy. For this baseline study, we directly adopted the information content (IC) measure as described by *Rodgers* [1996] and applied it at each retrieval level. We used a simple formula reasonably bounding the number of channels per level as well as the total number of channels.

[15] Following *Rodgers* [1996] [see also *Bennett et al.*, 1999], the IC may be viewed as the information gained by including a measurement or, alternatively, as the corresponding incremental reduction in uncertainty. It is a scalar measure, H , expressed as the logarithm to base two (units of bits) of the “ratio” of prior to posterior error covariances in the form

$$H = 1/2\{\log_2|\mathbf{S}_a\mathbf{S}^{-1}|\}. \quad (2)$$

In equation (2) \mathbf{S}_a is the a priori error covariance matrix and \mathbf{S} is the retrieval error covariance matrix defined by

$$\mathbf{S} = [\mathbf{S}_a^{-1} + \mathbf{K}^T\mathbf{S}_e^{-1}\mathbf{K}]^{-1}, \quad (3)$$

where \mathbf{S}_e is the measurement error covariance matrix and \mathbf{K} is the forward model operator, or weighting matrix, introduced above in section 2.2. The specification of \mathbf{S}_a , \mathbf{S}_e , and \mathbf{K} for this study is detailed in section 2.4 below. In implementing the selection, we presorted the IASI channels into the retrieval levels based on the peak of weighting functions (rows of matrix \mathbf{K}) associated with them; that is, each channel was allocated to that level where its weighting function peaks. This presorting by level acts to distribute the weighting functions such that each retrieval level safely receives a sufficient number of channels. Moreover, the IC selection processing time is reduced since the number of channels in each layer is small compared to computing on all channels at once. Then at each level (43 for temperature, 28 for humidity) H was computed by updating the retrieval error covariance matrix from the calculation of \mathbf{S} in the previous step [cf. *Rodgers*, 1996]. The channel with the greatest H value, H_{\max} , is retained for the retrieval and removed from subsequent calculations of H_{\max} repeating the procedure for one channel less. The selection via H_{\max} stops for a given level i after N_i channels are determined, where N_i is computed by the heuristic formula

$$N_i = \min\{\min[n_i, \max((f * n_i), n_{\text{thres}})], n_{\text{max}}\}. \quad (4)$$

In (4), n_i is the total number of channels available at the level (corresponding to the number of weighting functions peaking there), f is a fraction parameter, n_{thres} is a threshold parameter, and n_{max} is a parameter for the maximum number of channels allowed. The free parameters f , n_{thres} , and n_{max} in (4) are used to enforce a suitable target number of channels both per level and in total. For this study we used for temperature retrievals below/above 100 hPa $f = 0.07/0.07$, $n_{\text{thres}} = 25/15$, and $n_{\text{max}} = 40/25$ and for humidity retrievals $f = 0.07$, $n_{\text{thres}} = 15$, and $n_{\text{max}} = 50$ throughout, respectively. These parameters were selected, after tests with many different parameter scenarios, so that (1) the final number of channels obtained would not exceed 700 ($\sim 8\%$ of total number), (2) all retrieval levels are properly represented with somewhat more weight on tropospheric heights, and (3) the vertical distribution of channels is smooth (small gradient in the number of channels associated with adjacent levels).

[16] Figure 2 illustrates the outcome of the IC selection, for both temperature T and humidity q , by showing the IC measure H (incremental IC in bits) as a function of wave number for those channels, which have been selected. $\mathbf{K}_T = \partial\mathbf{T}_B/\partial\mathbf{T}$ and $\mathbf{K}_q = \partial\mathbf{T}_B/\partial\ln q$ were evaluated for a standard midlatitude summer atmosphere in this case, which served as the standard a priori atmosphere in this study. It is generally sensible to base the computation of \mathbf{K}_T and \mathbf{K}_q for the selection on a priori temperature and humidity information. Separate channel sets were prepared for T and q (the one for T using \mathbf{K}_T in (3), the one for q using \mathbf{K}_q) as we retrieve these parameters separately in this baseline study. The number of channels eliminated by this step is around 4500 ($\sim 87\%$ of the channels on input), leaving ~ 600 – 700 channels based on highest IC per level.

[17] Though the numbers N_i (equation (4)) are not particularly high, the computation of H_{\max} , required N_i times per level, is computationally demanding. For example, suppose that for humidity retrievals, 100 channels peak at level

30 (520 hPa). This would require a total of $\sum_{n=0}^{14} (100-n)$ calculations of IC or, in other words, H_{\max} is realized 1395 times at level 30. Since this step can be computationally intensive for levels with many channels, the channel selection was carried out only for the U.S. standard climatological profiles and is not foreseen to be done in this way for individual retrievals in large-scale application (these would use a prescribed channel set closest to current conditions, e.g., based on climatological prior information such as from the CIRA86aQ_UoG model [Kirchengast *et al.*, 1999]). We have, however, also successfully explored simplified faster information content measures [Weisz *et al.*, 2001; unpublished manuscript].

2.3.4. Channel clustering

[18] After the IC step, we are left with <10% of the original channels. As Figure 2 indicates, many of the channels are in tight groups (as in the CO₂ absorption bands), and yet others span across the water vapor vibration-rotation band. We seek to further reduce redundant information, while at the same time suppressing instrumental noise, by creating single pseudochannels in case clusters of four neighboring channels occur at a single retrieval level. An average over the measurement values and weighting functions of channels is performed in such clusters, and the error values involved in \mathbf{S}_e are reduced by a factor of ~ 0.6 to reflect the noise reduction due to averaging (since the four channels are correlated there is less error reduction than by $1/\sqrt{4}$). Each pseudochannel thus replaces four individual channels (reducing the number of channels by three) and exhibits improved error characteristics. Restricting clustering to single retrieval levels ensures that the brightness temperature differences among the neighboring channels are small and that the vertical resolution is not blurred. In general, clustering reduces measurement redundancy in “atmospheric window” regions or in regions displaying spectral homogeneity. Clustering over more than 1 cm^{-1} (more than four channels) was not performed in order to ensure that the weighting functions involved are similar, particularly in the 1600 cm^{-1} H₂O band and along the wings of the CO₂ bands centered near 650 and 2300 cm^{-1} . This final step of the channel reduction procedure typically produces ~ 10 – 15 pseudochannels, which are indicated by asterisk symbols in Figure 2. The number of channels available for the retrieval algorithm is thus ~ 600 ($\sim 7\%$ of the total). Moderate room for improved clustering exists in making the handling of cluster size more flexible (e.g., size variable between two and four to eight channels dependent on supply of cluster blocks at any level involving sufficiently similar weighting functions).

2.4. Retrieval Algorithm

[19] We approach the inverse problem associated with (1), the retrieval of temperature and humidity profiles x from brightness temperature measurements \mathbf{y} , by the concept of Bayesian optimal estimation described in detail by Rodgers [2000]. Since the problem of interest is moderately nonlinear, we chose an iterative optimal estimation of the form

$$\mathbf{x}_{i+1} = \mathbf{x}_a + \mathbf{S}_i \cdot \mathbf{K}_i^T \cdot \mathbf{S}_e^{-1} \{ [\mathbf{y} - \mathbf{F}(\mathbf{x}_i)] + \mathbf{K}_i \cdot (\mathbf{x}_i - \mathbf{x}_a) \}, \quad (5)$$

where subscript i is the iteration index, \mathbf{x}_a is an a priori profile (for temperature or humidity), \mathbf{S}_i is the retrieval error

covariance matrix defined by (3), \mathbf{S}_e is the measurement error covariance matrix, and the other quantities are as defined earlier. The optimization scheme expressed by (5) is usually termed Gauss-Newton method and provides a reliable maximum a posteriori (MAP) estimate for “small residual” inverse problems as the one dealt with here [Rodgers, 2000]. In applying (5), the iteration was initialized with $\mathbf{x}_0 = \mathbf{x}_a$ and state estimate, \mathbf{x}_i , measurement estimate, $\mathbf{y}_i = \mathbf{F}(\mathbf{x}_i)$, weighting matrix, $\mathbf{K}_i = \partial \mathbf{F}(\mathbf{x}) / \partial \mathbf{x}|_{\mathbf{x}=\mathbf{x}_i}$, and retrieval covariance estimate, \mathbf{S}_i , were updated at each iteration step until convergence (or a maximum number of 12 iterations) was reached. Convergence was determined based on the scalar “cost function” measure

$$\chi_i^2 = [\mathbf{y} - \mathbf{F}(\mathbf{x}_i)]^T \mathbf{S}_e^{-1} [\mathbf{y} - \mathbf{F}(\mathbf{x}_i)] + (\mathbf{x}_i - \mathbf{x}_a)^T \mathbf{S}_a^{-1} (\mathbf{x}_i - \mathbf{x}_a). \quad (6)$$

If χ_i^2 is less than N_{chan} , the number of channels (approximately corresponding to the number of degrees of freedom involved [Rodgers, 2000]), then convergence is considered obtained when the criterion $(\chi_{i+1}^2 - \chi_i^2) < 0.1N_{\text{chan}}$ is met and the profile with the minimum χ^2 value (either \mathbf{x}_i or \mathbf{x}_{i+1}) is retained. In the event a maximum of 12 iterations is used up without convergence as defined or if χ^2 values start to re-increase at $\chi^2 > N_{\text{chan}}$, the profile \mathbf{x}_i with the minimum χ^2 value is retained and properly flagged. Convergence is usually obtained with one to three iterations for temperature and two to four iterations for humidity retrievals. The computationally most demanding part in the estimation scheme is the calculation of \mathbf{K}_i (dimension $N_{\text{chan}} \times$ number of retrieval levels), which must be performed at each iteration step (by the RTIASI model). Effective channel reduction is of key importance to render this efficient.

[20] The a priori error covariance matrix (\mathbf{S}_a) reflects the uncertainty in our knowledge of how close the a priori profile \mathbf{x}_a is to the “true” profile x we desire to estimate. In order to reflect the typical smooth character of a priori profiles, we use an autoregressive model variant and adopt \mathbf{S}_a to be nondiagonal such that there exists interlevel correlation and the nondiagonal components fall off exponentially from the diagonal, i.e.,

$$\mathbf{S}_a(i, j) = \sigma_i \sigma_j \exp\left(\frac{-|z_i - z_j|}{L}\right). \quad (7)$$

In (7), σ_i and σ_j are the standard deviations of the a priori error covariance matrix, z is height, and L is the correlation length. For temperature, $L = 3 \text{ km}$, and the standard deviations are assumed to grow linearly in log pressure from 2 K at the surface to about 14 K at the top of the model (0.1 hPa). For humidity, $L = 1 \text{ km}$, and we assume a similar type increase in standard deviation from surface to 400 hPa (linear from 25 to 40% uncertainty). Above 400 hPa, a constant value of 40% is used. For application to the smooth climatological profiles used in the present study, this specification of covariances is generally conservative.

[21] The measurement error (or noise) figures were obtained from the best available current noise model for IASI level 1c data (P. Schuessel, EUMETSAT, private communications, 2000). The diagonal elements of \mathbf{S}_e were set to the (squared) noise figures, the off-diagonal elements

set to represent interchannel correlation up to the third neighboring channel required to account for the apodization process involved in the spectrum. Before using the noise figures, the standard noise figures (referring to a background scene at 280 K) were scaled to the actual brightness temperature of each channel (i.e., if this is colder than 280 K the scale factor is higher than unity). It is sufficient to determine this scaling from forward modeled a priori information. Typical instrument measurement noise values range between 0.1 and 0.5 K with a marked increase for wave numbers above 2500 cm^{-1} , one major reason why we limited the wave number range to $<2500\text{ cm}^{-1}$ (see subsection 2.3.1). In addition, we roughly account in \mathbf{S}_e for forward model (RTIASI) deficiencies by adding for all channels 0.2 K to the measurement errors (J. Eyre, The Met. Office, Bracknell, U.K., private communications, 2000). Besides implementing \mathbf{S}_e according to this formulation, each simulated measurement vector y was superposed by a randomly generated noise vector statistically consistent with the formulation of \mathbf{S}_e (except for the forward model error component, which need be ignored when generating noise in y).

[22] Dependent on the quality of the a priori profile, the first or the first two iteration steps may need special aid with convergence due to linearization errors, which is often dealt with in extending the Gauss-Newton scheme to the Levenberg-Marquardt scheme [e.g., Rodgers, 2000; Rieder and Kirchengast, 1999]. We utilized the more simple but for the present purpose equivalently effective extension introduced by Liu *et al.* [2000], termed ‘‘D-rad’’ method. Leaving (5) unchanged, just \mathbf{S}_e is modified in its diagonal according to

$$\mathbf{S}_e(m, m) = \max \left[\frac{(y(m) - y_i(m))^2}{\alpha}, \sigma_i(m)^2 \right], \quad (8)$$

where i is the iteration index, $y(m)$ is the measurement value of channel m , $y_i(m) = F_m(\mathbf{x}_i)$ is the forward-modeled measurement, α is a (free) control parameter set to 10 for this study, and $\sigma_i(m)^2$ is the variance of measurement noise for channel m (the original $\mathbf{S}_e(m, m)$ values). Liu *et al.* [2000] found the ‘‘D-rad’’ extended Gauss-Newton algorithm to perform equally well or better than the Levenberg-Marquardt algorithm in aiding convergence when a poor initial guess profile was given. It also performs well in the present context.

3. Results and Discussion

[23] Several examples are shown in order to demonstrate the performance properties of applying an optimal estimation retrieval algorithm to a reduced simulated set of high spectral resolution measurements. For the tropical climatology example discussed below, the number of channels after the reduction steps according to section 2.3 were 651 and 534 for temperature and humidity, respectively.

[24] First it is instructive to examine, for both temperature and humidity, the vertical-derivative-of-transmittance functions (rows of matrix $\partial\tau/\partial\ln p$, which has dimensions number of channels \times number of levels), the weighting functions (rows of matrix \mathbf{K} , which has dimensions number of channels \times number of levels), and the averaging kernel

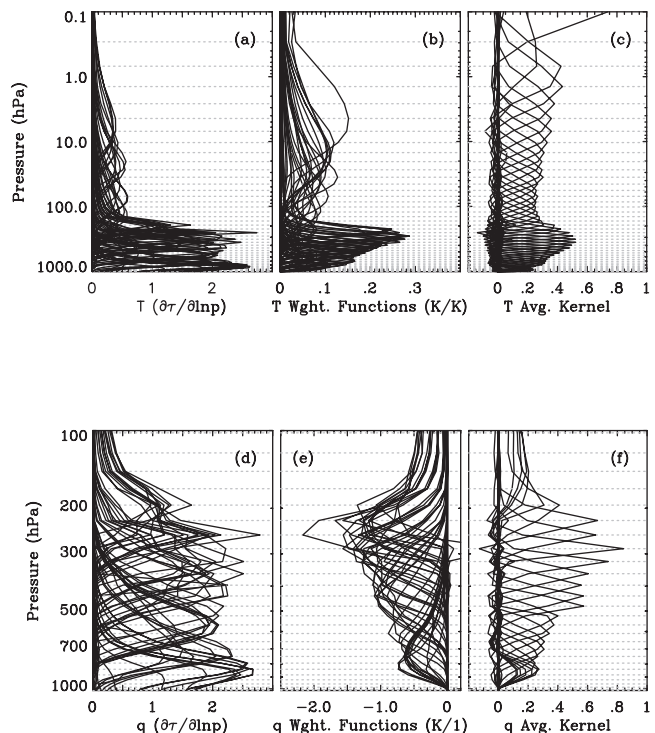


Figure 3. (a, d) Vertical-derivative-of-transmittance functions, $d\tau/d\ln p$, (b, e) weighting functions, and (c, f) averaging kernel functions for Temperature, T , and humidity, q , respectively. For highlighting the nonuniform level spacing used, the grid levels are indicated as dashed gray lines. Only every eight channel is displayed for clarity in Figures 3a, 3b, 3d, and 3e.

functions (rows of matrix $\mathbf{A} = \mathbf{S}\mathbf{K}^T\mathbf{S}_e^{-1}\mathbf{K}$, which has dimensions number of levels \times number of levels), respectively. (We deliberately do not term rows of $\partial\tau/\partial\ln p$ ‘‘weighting functions’’ to avoid potential confusion with the rows of \mathbf{K} , the Jacobians, which are termed weighting functions in our notation [Rodgers, 2000]).

[25] The vertical-derivative-of-transmittance functions represent the classical kernel of the ‘‘atmospheric integral term’’ of the radiative transfer equation. Figure 3 illustrates them both for temperature (total transmittance) (Figure 3a) and humidity (H_2O -only transmittance), (Figure 3d). We do not directly utilize them in this study but shown them for reference, especially in order to highlight the difference to the weighting functions (Figures 3b and 3e).

[26] The weighting functions quantify the sensitivity of measured values y to the state \mathbf{x} , while the averaging kernel functions express the sensitivity of the retrieved state \mathbf{x}_i (estimated via (5)) to the true state x and give with the width of their main peak at half-maximum a measure of the vertical resolution of the retrieved profiles [Rodgers, 2000]. Figures 3b, 3c, 3e, and 3f illustrate the vertical distribution and magnitude of the weighting and averaging kernel functions and indicates where the retrieval performance is expected to be good or degraded. Note that for humidity $\mathbf{K} = \partial\mathbf{T}_B/\partial\ln q$, thus the units are K/1. The retrieval grid is indicated by grey dashed lines in order to highlight its nonuniform spacing, which increases close to

linearly with height (by a factor of ~ 3 from 900 to 200 hPa, where it is ~ 1 km, and by a factor of ~ 4 from 200 to 1 hPa, respectively).

[27] The nonuniformity needs to be taken into account especially when interpreting the height dependence of the magnitudes of weighting and averaging kernel functions independent of the chosen grid. For this purpose the functions' values should be considered rescaled (divided) by the linearly increasing spacing in order to be representative of a uniform grid. Such scaling implies a significant increase of the magnitudes at lower heights relative to the ones at greater heights while the widths of function peaks are not changed much as the local non-uniformity across any single peak is linear and weak in the present case. Strictly speaking, the complete matrices \mathbf{K} and \mathbf{A} should be transformed to a uniform grid by utilizing the generalized inverse of the matrix interpolating the state x to the uniform grid [Rodgers, 2000].

[28] The weighting functions show highest peak magnitudes in the middle to upper troposphere (~ 500 – 200 hPa) implying greatest sensitivity of the measurements to the state x at these levels, while the sensitivity to the atmospheric state in general (independent of the chosen grid) is slightly greater in the lower troposphere. The averaging kernel functions also indicate rather sharp resolution of retrieved profiles (~ 1.5 – 2 km) in the 500 – 200 hPa region. Together this strongly indicates the potential of IASI measurements to monitor the upper troposphere both in thermal structure and moisture, at least in clear air. In contrast, the boundary layer (>900 hPa) and equatorial tropopause region (near 100 hPa) appear to be probed, at reasonable resolution as expressed by the chosen grid, with comparatively degraded sensitivity as indicated by the smaller magnitudes of weighting functions in these regions. Throughout the stratosphere, reasonable sensitivity is indicated up to the stratopause (~ 1 hPa) for temperature, while reasonable sensitivity to humidity is limited to below ~ 200 hPa (thus the retrieval domain for humidity was restricted to below 100 hPa). Above these levels, no significant weighting function peaks exist, the resolution is rather low, and the retrieval is dominated by a priori information. As we deal with thermal infrared sounding, the characteristics of matrices \mathbf{K} and \mathbf{A} (and $\partial\tau/\partial\ln p$) are significantly influenced by the type and concentration of interfering cloud and aerosol particles if these are present in the sensor's field of view. While this sensitivity complicates temperature and humidity profiling, it can be exploited to extract valuable information on clouds. In this study we assumed cloud free field of views.

[29] "Baseline case" retrievals of temperature T and humidity q were carried out using a standard midlatitude summer profile as a priori profile and simulated measurements from a standard tropical profile, superposed with noise according to \mathbf{S}_e . For the T retrieval the corresponding q profile was assumed perfectly known in this case and vice versa. The results are illustrated in Figure 4. Besides the final retrieval results, the results of intermediate retrieval steps (intermediate \mathbf{x}_i values in (5)) are shown in order to highlight the improvement with subsequent iterations, particularly where the initial step performs poorly (e.g., near the tropopause).

[30] For temperature, differences from the "true" profile initially vary up to 20 K at the tropopause, 5 K near the

surface, and 3–10 K in the stratosphere. After three steps (two iterations) the final temperature differences in most of the troposphere and stratosphere are less than 1 K. Near 100 hPa, temperature differences are reduced to ~ 4 K. The peak difference at these heights indicates the difficulty to resolve the sharp equatorial tropopause structure, which falls already above the best performance region below ~ 200 hPa discussed earlier. The retrieved RMS error estimates (square root of diagonal of \mathbf{S}_i , (3)), Figure 4c, are consistent with the actual differences, Figure 4b, in the troposphere but more conservative than those in the stratosphere. The reason is that the "smoothing error" component [Rodgers, 2000] is estimated rather conservatively by (3) in the given case, since the adopted a priori error covariance matrix represents an ensemble of profiles with more spatial variability of errors than contained in the smooth a priori profile used in the retrieval. Generally, the RMS error magnitude is small where the weighting functions (Figure 3b) are strong and vice versa.

[31] For humidity, improvement upon the initial step result is also significant, and the final retrieval is obtained after the first iteration (in this baseline case). A linear-log plot is used below 500 hPa, and a log-log plot is used above this height to best visualize the results despite the exponential decay of specific humidity with height. According to Figure 4e the initial difference of the a priori profile ranges from $\sim 25\%$ near the surface to 50% near 250 hPa. Throughout the troposphere, the retrieved humidity profile is within 10% of the "actual" profile, indicating the potential of IASI to furnish rather accurate humidity information given an accurate a priori temperature. Regarding the retrieved RMS error estimate, Figure 4f, the most salient feature is again the dependence of accuracy on measurement sensitivity (illustrated by the weighting functions in Figure 3e). As for temperature, also the humidity error estimate is conservative, since the a priori error covariance matrix was not specifically tailored to the midlatitude summer climatological profile but is rather reflecting a broad ensemble of thermodynamic profiles including more variable ones. It should be noted that only the diagonal component of the retrieval error covariance matrix is shown in Figures 4c and 4f, while a more detailed error analysis recently worked out (Weisz et al., unpublished manuscript, 2001) also examines the error correlation structure.

[32] While Figure 4 has illustrated a baseline case where we prescribed the actual q/T profile for the T/q retrieval (which is idealistic), it is of practical interest to learn how sensitive the retrieved T/q profiles are to uncertainties in the prescribed q/T profiles. Related to this we performed preliminary tests with a retrieval algorithm jointly retrieving T and q , both stacked into state x in (5). Also, all the other relevant quantities (especially \mathbf{S}_a , \mathbf{K}) were extended accordingly, and different channel subsets were considered. Repeating the baseline case discussed above in this joint retrieval mode indicated that the humidity sensitivity prevented the preliminary scheme from reaching convergence in the tests run. Thus we quantitatively studied the sensitivity of T/q retrievals to prescribed q/T profiles in applying perturbations to the prescribed profiles and observing the effects on the retrievals.

[33] Results for three representative perturbations of q/T profile are shown in Figure 5: two systematic plus/minus

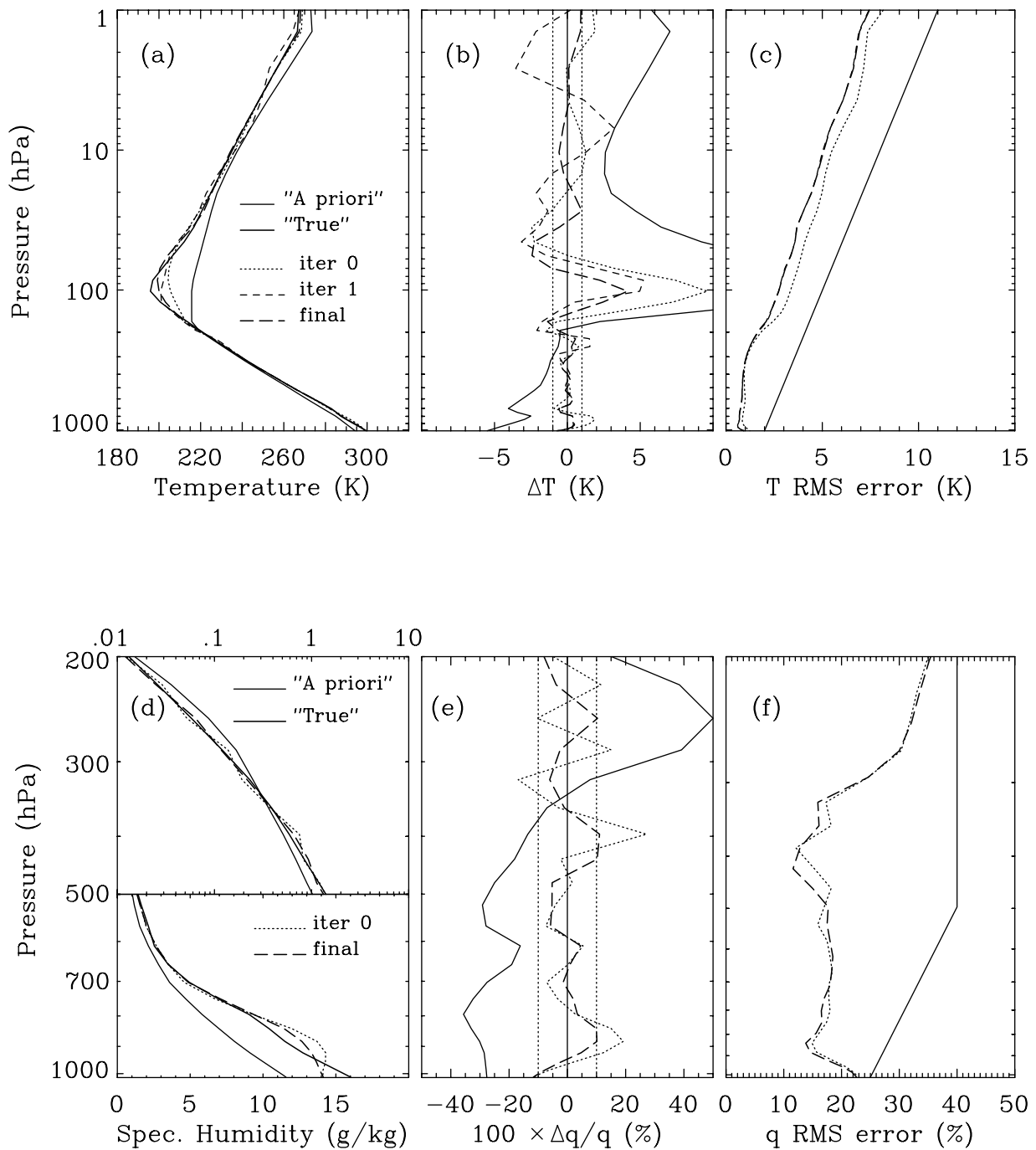


Figure 4. (a) IASI temperature retrieval and iteration results, using a standard midlatitude summer a priori profile and standard tropical “true” profile. (b) Temperature difference profiles from “true” profile. (c) Square root of the diagonal of temperature error covariance matrices. (d) Humidity retrieval in log-log coordinates for 200–500 hPa range and linear-log coordinates for 500 hPa–surface range. (e) Relative difference profiles from “true” profile. (f) Square root of the diagonal of humidity error covariance matrices.

perturbations and one randomly generated profile realization consistent with the q/T a priori covariance matrix used. The midlatitude summer profile was used as a priori profile in all cases. Figures 5a and 5b indicate that the retrieved temperature is quite robust when subjected to large (even somewhat unrealistic) uncertainties in the prescribed q profile. For both the systematic $\pm 30\%$ uncertainties and

the relatively large uncertainties in the realization profile, the retrieval error stays within 3 K in the troposphere (except toward the surface) and is not degraded in the stratosphere. Note that systematic humidity deviations produce systematic temperature errors in the troposphere: the retrieved temperature is consistently warmer/cooler than the “true” one if the prescribed humidity is too moist/dry.

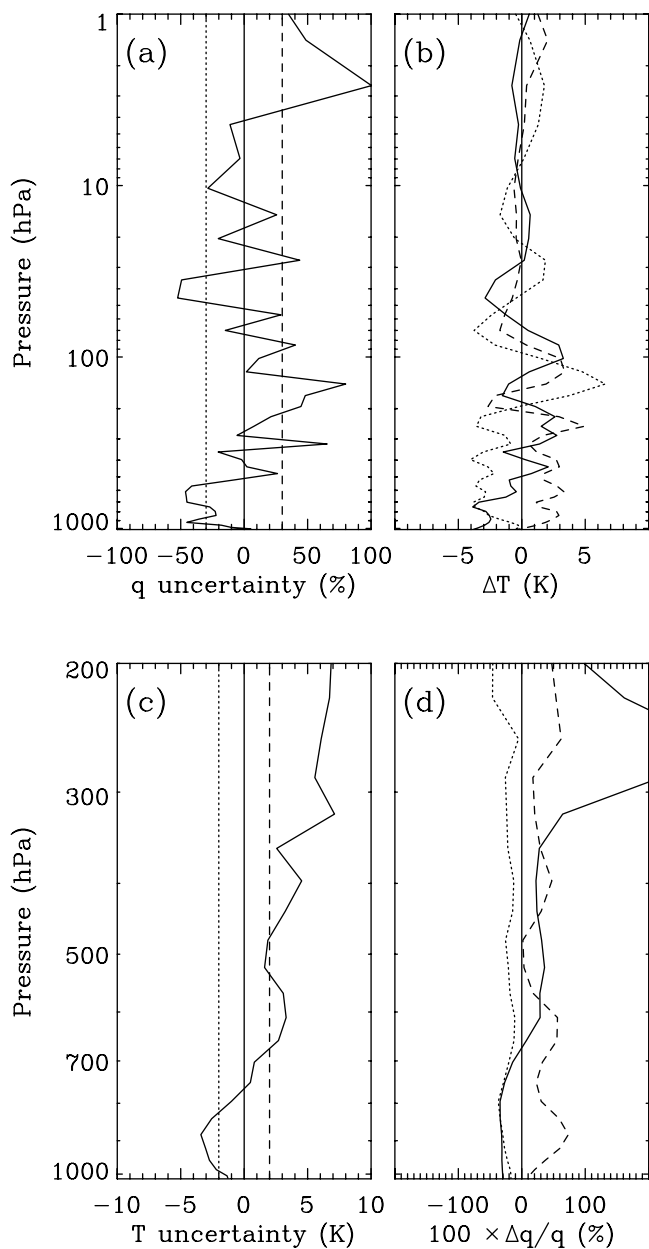


Figure 5. Sensitivity of (a, b) temperature retrievals and (c, d) humidity retrievals to (a) prescribed humidity (Figure 5a) and prescribed temperature (Figure 5c) uncertainties, respectively. The retrievals are shown as absolute difference profiles from “true” profile for temperature (Figure 5b) and relative difference profiles from “true” profile for specific humidity (Figure 5d), respectively.

[34] Humidity retrievals are much more sensitive to perturbations in the prescribed temperature profile as Figures 5c and 5d indicate. For systematic T perturbations of ± 2 K, the q retrievals are biased by about ± 20 – 30% . Below 800 hPa the sensitivity is significantly more pronounced with the retrieval difference exceeding 60% for a $+2$ K perturbation. The (rather unrealistic) random realization profile produces big differences in the upper troposphere, where the temperature perturbation exceeds 5 K. The results underscore the requirement for accurate a priori temperature information

(uncertainties less than ~ 2 K) for retrieving both temperature and humidity (e.g., from a comprehensive library of profiles or a ≤ 24 hours weather prediction model forecast).

[35] A further sensitivity of interest is that of the retrieved profile to the a priori profile used. It indicates how a priori profile errors may alter the retrieval. Figure 6 displays, for both temperature and humidity, results on these sensitivities invoking the different extratropical U.S. standard atmosphere

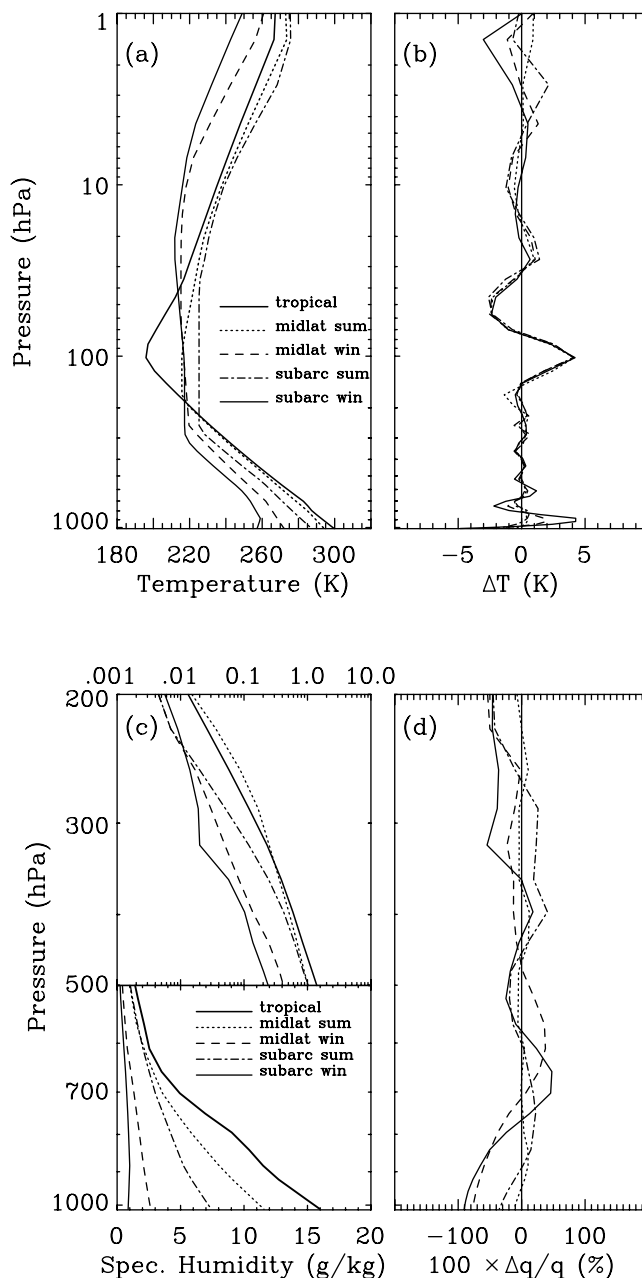


Figure 6. (a and b) Sensitivity of temperature retrievals and (c and d) humidity retrievals to different a priori temperature (Figure 6a) and humidity (Figure 6c) profiles, respectively. The retrievals are shown for temperature (Figure 6b) and specific humidity (Figure 6d) in the same manner as in Figure 5. Linestyles in Figure 6b same as in Figure 6a and in Figure 6d as in Figure 6c, respectively.

profiles as a priori profiles for retrieving the tropical profile. The prescribed profiles are assumed known in these sensitivity tests. In the troposphere and lower stratosphere, the temperature retrievals arrive at a solution that is very similar for all cases. We begin to see the solutions diverge above ~ 30 hPa where the uncertainty in the a priori profiles increases (as reflected in the prescribed a priori error covariance matrix (Figure 4c)). These results indicate that the T retrieval is rather robust against a priori profile deviations. By varying the channel set used (not shown) the differences in the solution can vary by up to 2 K in the middle to upper stratosphere (e.g., when the midlatitude winter based channel set is used to retrieve a tropical temperature profile). The channel sets produced for the different standard states according to section 2.3 differ since shape and magnitude of the weighting functions for individual channels are a function of water vapor amount and, to a lesser degree, of temperature. For the q retrievals, the a priori profile plays a much more prominent role and initial profiles too far apart (best indicated by the results for the much too dry winter profiles) destroy convergence. In our example, it can be seen (Figure 6d) that the a priori profile needs to be about as good as the subarctic summer humidity profile in order to achieve an accuracy within 25% of the tropical profile.

4. Summary and Conclusions

[36] In this paper we have presented an algorithm to retrieve temperature and humidity from measurements made by the Infrared Atmospheric Sounding Interferometer (IASI), scheduled for launch aboard the METOP-1 satellite in 2005. The algorithm is also applicable for retrievals from other similar high-resolution spectra. Main features are a sensible channel reduction procedure followed by an iterative optimal estimation. A four-step procedure was introduced for down-selecting channels, which includes: removal of channels $< 4 \mu\text{m}$ potentially contaminated by solar radiation, “foreign” gas elimination, information content based channel reduction, and channel clustering. This procedure results in (1) reducing the total channel number (> 8000 in case of IASI) by about 90–95% thus increasing computational efficiency of the retrieval process without appreciably compromising accuracy, (2) effectively removing redundant information (e.g., due to multiple absorption bands all supplying sensitivity for similar heights or in atmospheric windows), (3) preserving channels whose weighting function peaks smoothly span almost all retrieval levels, and (4) reduce retrieval uncertainties by removing channels where significant emissions by nonretrieved and nonuniformly mixed gases (e.g., O_3) are present.

[37] An iterative linearized optimal estimation retrieval algorithm for moderately nonlinear problems was employed for deriving temperature and humidity profiles from the selected subset of simulated measurements. U.S. standard climatological profiles were used to supply background a priori profiles as well as a “true” profile (a standard tropical profile) for demonstrating the retrieval performance of the algorithm including various sensitivity tests. The retrieval of temperature performs quite well (less than 1 K difference from “true”) throughout most of the troposphere and mid stratosphere if the prescribed humidity profile is well known (within 10%). Humidity retrievals are within 10% of the

“true” humidity profile throughout most of the troposphere up to 200 hPa if the prescribed temperature profile is well known (within 1 K). Convergence is typically reached within 1–3 iterations for temperature and 2–4 iterations for humidity.

[38] Temperature retrievals appear to be quite robust against uncertainties in prescribed humidity (up to about 20–40% uncertainty). Humidity retrievals are significantly more sensitive, and prescribed temperature uncertainties should stay within 2 K. Varying the a priori temperature profile (while keeping humidity fixed) led to temperature retrievals, which agreed with one another within 1 K at most heights between 700 and 30 hPa. Varying the a priori humidity profile (while keeping temperature fixed) in humidity retrievals led to differences of the order of 30–50% from the “true” profile when using inappropriate a priori profiles (e.g., dry winter profiles). This indicates that for supplying a fair a priori state, one should best use a suitable profile from a comprehensive library of profiles or a short-term model. Typically the a priori errors would then be smaller than what was adopted here.

[39] The results of this baseline study provide clear guidance for further advancements. Our current and planned future work includes: (1) Improving the channel reduction procedure, especially toward using a simplified information content measure enabling more efficient selection, (2) Improving the retrieval algorithm to fully realistic conditions either via a “joint retrieval mode” (stacking both temperature and humidity profiles into one state vector) or a “sequential mode” (based on a chain of subsequent temperature and humidity retrievals), (3) a thorough analysis of the retrieval process based on a Bayesian error analysis and characterization formalism, (4) application of the algorithm under realistic IASI sounding geometry to high resolution weather analyses in order to test retrieval performance on realistic mesoscale variability, and (5) modifications and optimizations focused on high-quality retrieval of upper tropospheric humidity and sea surface temperature. The results obtained so far strongly indicate that the high spectral resolution measurements from IASI indeed have high potential to significantly outperform current operational sensors in temperature and humidity profiling and that they may become a future key database for the much needed monitoring of climatic changes in the thermal structure of the atmosphere and especially the moisture distribution of the middle and upper troposphere.

[40] **Acknowledgments.** We thank M. Matricardi (ECMWF, Reading, U.K.) for kindly providing (an early version of) the RTIASI model and related valuable advice. We are grateful to P. Schluessel (EUMETSAT, Darmstadt, Germany) for providing a consolidated version of the RTIASI model (which is a property of EUMETSAT) and the recent IASI level 1c noise model as well as for useful comments on the manuscript. Furthermore, we like to thank J. Eyre (The Met. Office, Bracknell, U.K.) for helpful scientific discussions. The work was financially supported by the START research award of G. K. funded by the Austrian Ministry for Education, Science, and Culture and managed under Program Y103-CHE of the Austrian Science Fund.

References

- Bennett, V. L., A. Dudhia, and C. D. Rodgers, Microwindow selection for MIPAS using information content, in *Proceedings of the European Symposium on Atmospheric Measurements from Space*, pp. 265–270, Eur. Space and Tech. Cent., Noordwijk, Netherlands, 1999.

- Kidwell, K. B., *NOAA Polar Orbiter Data User's Guide*, NOAA/NESDIS Satellite Data Services Div., Washington D.C., 1986.
- Kirchengast, G., J. Hafner, and W. Poetzi, The CIRA86aQ_UoG model: An extension of the CIRA-86 monthly tables including humidity tables and a Fortran95 global moist air climatology model, *Tech. Rep. ESA/ESTEC No. 8/1999*, 18 pp., Inst. for Geophys., Astrophys., and Meteorol., Univ. of Graz, Austria, 1999.
- Kyle, T. G., Temperature sounding with a partially scanned interferogram, *Appl. Opt.*, *16*, 322–325, 1977.
- Liu, X., T. Scott Zaccheo, and J.-L. Moncet, Comparison of different non-linear inversion methods for the retrieval of atmospheric profiles, paper presented at the 10th Conference on Satellite Meteorology, Am. Meteorol. Soc., Long Beach, Calif., 2000.
- Matricardi, M., and R. Saunders, A fast radiative transfer model for simulation of Infrared Atmospheric sounding interferometer radiances, *J. Appl. Optics*, *38*, 5679–5691, 1999.
- Rieder, M. J., and G. Kirchengast, Physical-statistical retrieval of water vapor profiles using SSM/T-2 sounder data, *Geophys. Res. Lett.*, *26*, 1397–1400, 1999.
- Rodgers, C. D., Information content and optimisation of high spectral resolution measurements, in *Optical Spectroscopic Techniques and Instrumentation for Atmospheric and Space Research II*, vol. 2830, edited by P. B. Hays and J. Wang, pp. 136–147, Int. Soc. for Optical Eng., Bellingham, Wash., 1996.
- Rodgers, C. D., *Inverse Methods for Atmospheres: Theory and Practice*, 238 pp., World Sci., Singapore, 2000.
- Schmetz, J., W. P. Menzel, C. Velden, X. Wu, L. van de Berg, S. Nieman, C. Hayden, K. Holmlund, and C. Gejo, Monthly mean large scale analysis of upper troposphere humidity and wind field divergence derived from three geostationary satellites, *Bull. Am. Meteorol. Soc.*, *76*, 1578–1584, 1995.
- Smith, W. L., H. B. Howell, and H. M. Woolf, The use of interferometric radiance measurements for sounding the atmosphere, *J. Atmos. Sci.*, *36*, 566–575, 1979.
- Smith, W. L., H. E. Revercromb, H.-L. Huang, and R. O. Knuteson, Vertical sounding capabilities with high spectral resolution atmospheric radiation measurements—A demonstration with the High resolution Interferometer Sounder (HIS), in *High Spectral Resolution Infrared Remote Sensing for Earth's Weather and Climate Studies*, edited by A. Chedin, M. T. Chahine, and N. A. Scott, NATO ASI series, pp. 131–146, 1993.
- Spencer, R. W., and W. D. Braswell, How dry is the tropical free troposphere? Implication for global warming theory, *Bull. Am. Meteorol. Soc.*, *78*, 1097–1106, 1997.
- World Meteorological Organization, Statement of Guidance Regarding How Well Satellite Capabilities meet WMO User Requirements in Several Applications Areas, Tech. Document 922, Geneva, 1998. (Available at <http://www.wmo.ch/hinsman/Publications.html>)
-
- G. Kirchengast, Institute for Geophysics, Astrophysics, and Meteorology (IGAM), University of Graz, Universitaetsplatz 5, A-8010 Graz, Austria. (gottfried.kirchengast@uni-graz.at)
- J. A. Lerner, Fleet Numerical Meteorology and Oceanography Center, 7 Grace Hopper Avenue, Monterey, CA 93943, USA. (jeffrey.lerner@fnmoc.navy.mil)
- E. Weisz, CIMSS/Space Science and Engineering Center, University of Wisconsin, Madison, 1225 W. Dayton Street, Madison, WI 53706, USA. (elisabeth.weisz@ssec.wisc.edu)